ELSEVIER

Cement & Concrete Composites **17** (1995) 57–75

0958-9465/95/$9.50

Biaxial Fracture Tests on Concrete — Development and Experience

E. K. Tschegg,* M. Elser* & S. E. Stanzl-Tschegg†

*Institute for Applied and Technical Physics, University of Vienna, A-1040 Vienna, Austria
†Institute for Meteorology and Physics, University of Agriculture, A-1180 Vienna, Austria

(Received 15 April 1994; accepted 11 November 1994)

Abstract

Crack initiation and crack propagation in concrete buildings are mostly caused by a multi-axial stress field in the component. In order to simulate this realistic state of loading in the laboratory, a simple and handy apparatus for biaxial fracture tests was developed. Here, the principle of wedge splitting is applied and is extended by a hydraulic pressure device in order to realise the biaxial state of stress in the specimen.

In this device, rectangular-shaped notched specimens were broken under a defined biaxial state of stress with stable crack propagation. The load–displacement curves that were then measured permit a characterisation of the biaxial fracture behaviour of the material. Thus, the specific fracture energy and a nominal notch tensile strength can be easily determined from these graphs.

By means of this testing method the fracture-mechanical characteristics of concrete with diverse forms of aggregate (natural/crushed gravel) and under different storage conditions (wet/dry) were defined.

Construction details and considerations as to the testing facilities will be discussed. The various quantities influencing the biaxial fracture behaviour of concrete will be analysed in detail and will be discussed by means of a model.

Keywords: Concrete, biaxial tests, notched specimens, fracture behaviour, fracture energy, storage conditions, cracking stresses, strains.

1 INTRODUCTION

Cement-bound materials are mostly subjected to biaxial or multiaxial loading in the building construction. A precise knowledge of the behaviour of the material against cracking under the actual multiaxial loadings is absolutely indispensable for a secure and lasting design of constructions and structures in construction engineering and building construction. This is particularly important for buildings where exclusively unreinforced concrete is used. Several examples for unreinforced concrete buildings or parts of buildings are: surfacing with gun-applied concrete or dry-mix shot concrete (fibre reinforced concrete is also used) in construction of tunnels/galleries and massive concrete dams/water-power dams, respectively; dams and locks, as well as other offshore structures; recycling concrete for upper and lower base layers in road construction, as well as for horizontal sealings in industrial construction.

In recent decades the most varying mechanical material parameters (compression strength, flexural strength, Young's modulus, etc.) have been determined for concrete. In recent years the fracture behaviour of concrete has also been analysed and characterised. Most of these investigations on concrete were carried out under uniaxial loading. In comparison with this, few papers have considered the biaxial and multiaxial behaviour. Comprehensive and generally acknowledged older tests were carried out by Kupfer and co-authors[1,2] as well as by Nelissen[3] on prismatic specimens of different concrete qualities. In Ref. 4 the influence of the grain distribution of the aggregate on the strength behaviour of concrete and mortar was investigated on cylindrical specimens under biaxial loading. The results of all these early studies are reliable failure envelopes, stress–strain curves and a description of the macroscopic fracture appearance. Somewhat more recent experimental papers deal with triaxial or multiaxial loadings[5–9] and were carried out with

the intention of obtaining insights into stress–strain relationships, post-peak response and parameters for numerical material modelling.

All papers mentioned so far were concerned with investigations on smooth, unnotched specimens. When breaking these specimens, one or more fracture zones of different sizes could be observed. Of course the occurrence of several fracture zones influences the observed deformation behaviour during the test and then it is difficult to decide whether this influence is due to an actual change of the material behaviour or only to an interaction of fracture zones of different sizes. In this respect it is preferable to carry out biaxial or multiaxial tests on notched samples in order to characterise their fracture behaviour.[10] This has the advantage of obtaining only one fracture zone during the test and of thus creating clear and unambiguous relationships. Therefore, real material parameters are of great importance, in particular with numeric simulations where a structural response is already taken into account.

Investigations of the fracture behaviour on notched samples with biaxial or multiaxial loading are scarcely to be found in literature. In Refs 10 and 11 the influence of loading rate on the stress–strain behaviour of concrete under biaxial, compressive-impact, tensile loading is examined by means of a Split–Hopkinson-bar technique. The author used specimens that were notched on both sides. With a similar but somewhat modified apparatus Weerheijm and Reinhardt[10,12] also studied the influence of the rate effect on the pre-peak and post-peak behaviour of different qualities of concrete. They developed a model for this which confirms the values that were found experimentally.

In this study a biaxial homogeneous state of stress (compressive force σ_1; tension σ_2) is induced into a single-edge notched concrete specimen, as shown in Fig. 1. Thus, the fracture behaviour of concrete is investigated for different forms of aggregates (natural gravel or crushed gravel) with different loading stages after standard storage and dry storage.

2 TEST METHOD AND EXPERIMENTAL PROCEDURE

Specimen shape, as well as the construction of a new hydraulic loading device, was chosen according to similar criteria as already explained.[13] An extension of the RILEM three-point bend test[14] for biaxial fracture tests would have considerable disadvantages according to the opinion of the authors. Therefore, the splitting method for biaxial loading, according to Tschegg,[15–17] was developed further.

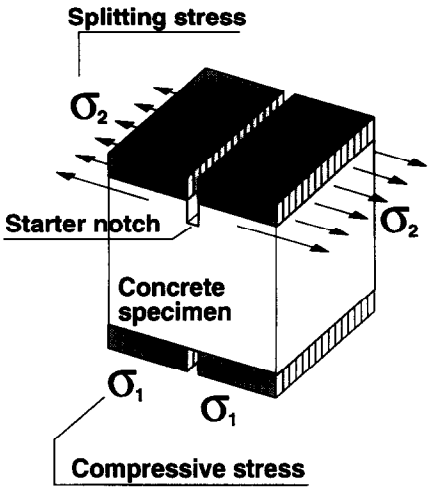

Fig. 1. Biaxial loading state of the specimen during the test (σ_1 = compressive stress, σ_2 = tension or splitting force, respectively).

2.1 Test equipment

2.1.1 Splitting test method for uniaxial testing

The basic set-up for biaxial loading is the wedge splitting test equipment for conventional, uniaxial application, according to Refs 15–17. This splitting method was adopted by other research groups[18–20] and was then published[18] as a new method.

In Fig. 2 the principle of uniaxial splitting is represented graphically. The cubic concrete specimen is provided with a rectangular groove in a plane of symmetry. A starter notch is introduced into the bottom of the groove. A wedge splitting test equipment (wedge, force transmission pieces with integrated needle bearings) is positioned in the groove in a simple manner and splits the specimens with stable crack growth due to the stiff construction and the hard behaviour of the loading device. The vertical force F_M of the compression testing machine (measurement by means of load cell) is split up vectorially, into a large horizontal force F_H (splitting force) and a smaller vertical force F_V, by means of a slender wedge. The values of F_H and F_V depend on the wedge angle α. The latter does not have any measurable influence up to a wedge angle of 15°, according to investigations carried out in Ref. 21. The measurement

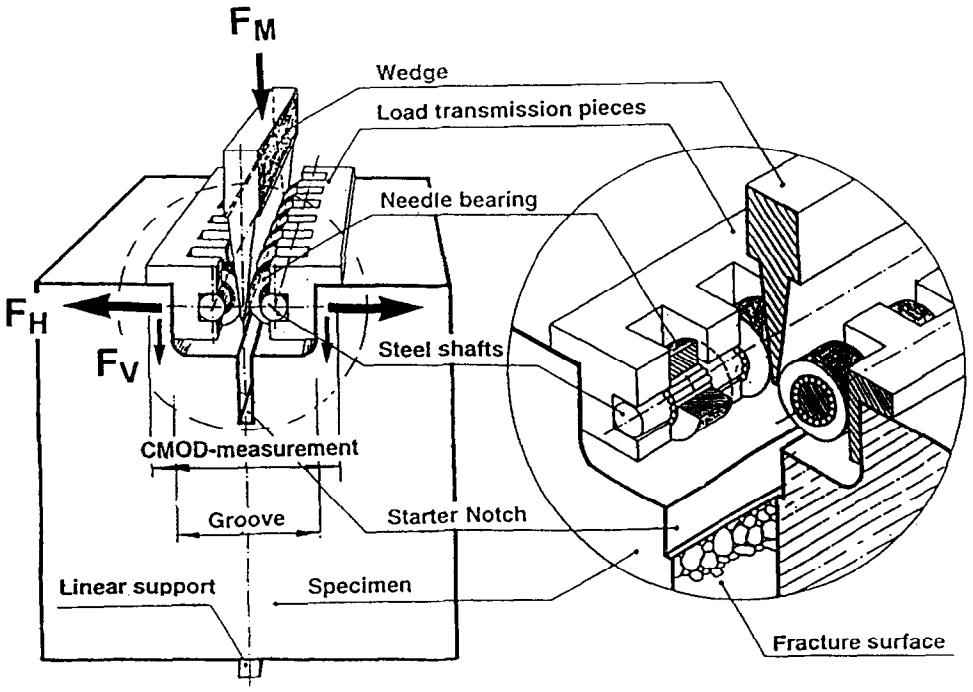

Fig. 2. Schematic representation of the splitting method[15] as well as details for the construction of the force transmission pieces.

error due to the frictional loss between wedge and force transmission pieces is minimised by needle bearings and lies in the negligible range of around 1%.[21]

Crack mouth opening displacement (CMOD) and force displacement are measured at both ends of the groove by means of electronic displacement transducers (LVDT-gauges), in order to detect a possible unsymmetric cracking. A simple measurement in the middle of the groove, as recommended in Ref. 18, has considerable disadvantages (see Ref. 17). The axes of the LVDTs are in the line of force application (wedge and needle bearings), i.e. force application and displacement measurement are in the same plane. LVDTs are mounted in a relatively simple way (see Fig. 3(b)), on a CMOD measurement device attached to the specimen by means of screw bolts. The cracking propagates in a rectilinear manner from the starter notch to the linear support. For both the uniaxial and the biaxial splitting process the so-called load–displacement curves for CMOD1 and CMOD2 are recorded as against the horizontal force F_H (calculated from F_M) until complete separation of the specimen. Thus, both the pre-peak and the post-peak behaviour (decreasing part of the load–displacement curve and softening-range, respectively) can be determined entirely. If these two curves deviated from each other by more than 20% of the area under the curve, the test was classified as not valid.

2.1.2 Biaxial loading system

This device[22] consists of a modified construction of the uniaxial splitting test[15–17] as its basic element (see Fig. 3(b)), as well as of an additional hydraulic compression loading unit (see Fig. 3(a)). The principle load transmission (wedge and needle bearings) remains unchanged, however, the needle bearings are integrated in load transmission slabs. Contrary to the specimen for uniaxial loading, the specimen for biaxial loading has no groove (Fig. 1). In order to introduce compression into the specimen homogeneously it is vital that the upper and lower surfaces of the specimen are parallel.

The biaxial state of stress (σ_1 and σ_2) is created by a vertical compressive force F_V and a horizontal splitting force F_H (see Fig. 1). The constant and homogeneous compressive stress σ_1 is obtained by a compressive loading unit (see Fig. 3(a)) consisting of two frames that are completely separated mechanically. These frames consist of tensile bars and flexurally rigid bars. Three hydraulic cylinders are mounted on each of the upper beams and each cylinder generates a maximum force of 111·3 kN. Via an oil pressure control, the desired σ_1-loading of the specimens, that

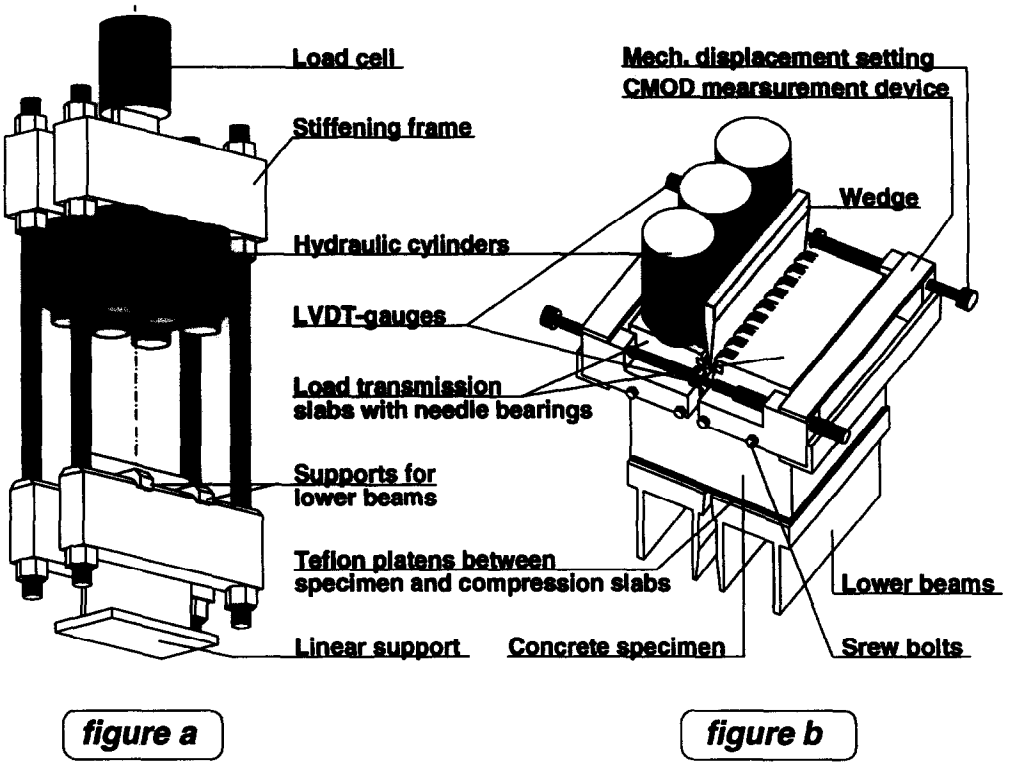

Fig. 3. Representation of the biaxial loading system: (a) both loading frames with three hydraulic cylinders each as well as a load cell and an auxiliary support; (b) specimen with load transmission slabs with integrated needle bearings and wedge as well as with lower beams and three hydraulic cylinders, CMOD-device with two LVDT gauges.

is to remain constant during the testing, can be controlled with sufficient precision. The great advantage of using a hydraulic system is that no stress relaxation can occur in the concrete during the splitting process because the hydraulic device is in operation during the entire time of the test procedure and keeps the desired pressure level constant.

In order to prevent the two halves of the compressive load application device (frame bars with half of the sample, CMOD-device with LVDT-gauges) (see Fig. 4(a)) from falling apart after the complete separation of the specimen, or when finishing the test, a thin flexible steel plate is inserted between the bottom of the specimen and the two lower beams. This plate does not influence the measuring operation or the measuring result in any way.

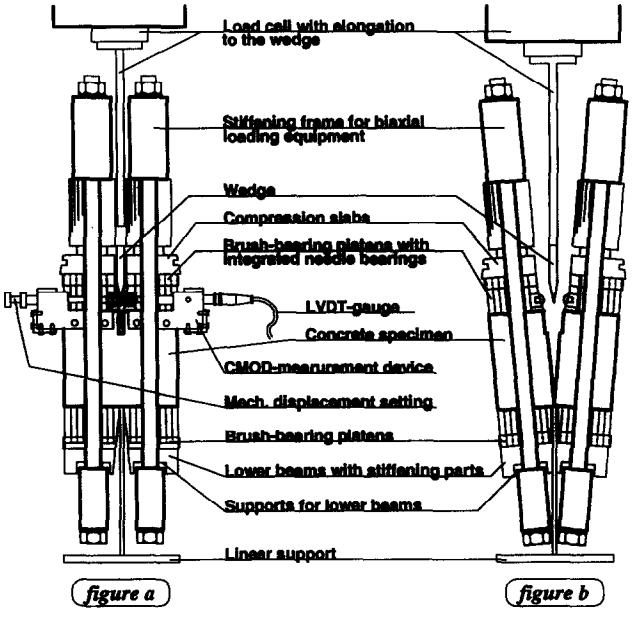

Fig. 4. View of the biaxial load system with integrated brush solution: (a) state before the experiment; (b) state after the experiment (without CMOD-device).

2.2 Introduction of uniform compression into the specimen

It is most important, for a constant and regular σ_1-stress distribution in the specimen, that the compression load is introduced homogeneously into the specimen. Both sides of the compression device (lower beams and load transmission slabs) influence the homogeneity of the load application to the specimen and, thus, also the homogeneity of the compressive stress distribution σ_1 in the specimen.

In contrast to the lower beams, the load transmission slabs do not need any additional stiffenings, since the transmission of the compressive stresses via the hydraulic cylinders does not occur in a concentrated manner, but is distributed over a large area on the load transmission slabs. In order to achieve a homogeneous compression distribution in the specimen, the most favourable positioning of the three hydraulic cylinders was determined by means of FE-methods.

Bending of the lower beams is minimised by additional stiffenings and by the most favourable arrangement of the bearings on the frame bar (see Fig. 3(a)).

By means of numerical and experimental methods we checked in how far a homogeneous introduction of compression could be achieved by construction means, as will be described below.

2.2.1 Analysis by means of FE-calculation

An ideal distribution is achieved if the cube is loaded via two slabs of infinite stiffness. In order to approach this condition, the stress distribution for the hydraulic load application device is calculated, using the FE-code ABAQUS in the same manner as calculated for a mechanical load application device.[23-25] A linear elastic 3D analysis for σ_1-loadings beween 20 and 80% of the compressive strength of concrete f_c is carried out by making a model for both the cube and all elements of the load application device. The results were used to improve the device until the σ_1-distribution around the fracture process zone was uniform with scattering less than 3%. The maximum scattering of the σ_1-distribution elsewhere was less than 10%, which was considered satisfactory, too.

2.2.2 Experimental check by means of pressure measurement foil

In order to determine the actual σ_1-distribution on the surface of the specimen, pressure measurement foils were inserted between the compression plates (or brushes) and the specimen at its upper side and lower side. These pressure measurement foils change their colour under different compression loading irreversibly in different ways. One example of such measurements of stress distribution is shown in Fig. 5(a). The pressure measurement foil was placed between the lower beam and the specimen (with cardboard inserted between pressure measurement foil and specimen). The result can be judged as being homogeneous (also in the boundary regions). In contrast to that a stress distribution decreasing towards the boundary region (Fig. 4(b)) was measured when using a laminated construction (see Figs 4(a) and (b)).

The results of the pressure foil measurements (Figs 5(a) and (b)) correspond very well to the calculated stress distributions calculated by means of the finite element (FE)-method.

In the following section (Test Series 2 and 3) the results of the pressure foil measurements will be discussed in greater detail.

2.3 Method to correct the transverse strain in concrete and steel

The different transverse strains of concrete ($\mu \cong 0{\cdot}2$) and steel ($\mu \cong 0{\cdot}3$) lead to an additional stress in the longitudinal direction of the specimen in the case of a large-area force transmission and, thus, cause a triaxial, inhomogeneous state of stress.

Various constructive measures can be taken or methods applied for the correction of the transverse strain. In order to select the optimum measure, a series of experimental tests were carried out.

2.3.1 Series 1: no measure

This test series serves as a comparison for further series where measures for the correction of the transverse-strain are taken. The concrete specimen is in direct contact with the steel surfaces of the pressure beams and the full constraint of the transverse strain becomes effective at the contacting surfaces between concrete and steel.

2.3.2 Series 2: laminated construction

Reference 1 suggests a solution of this problem that is generally acknowledged and frequently applied today: the design of the platens as a 'brush' construction (or 'laminated' construction). Figures 4(a) and (b) show how this measure was realised for the splitting method for biaxial loading. Investigation by means of pressure measurement foils at the bottom of the specimen (Fig. 5(b)) and on the upper surface showed that in the edges of force transmission the stress distribution decreases. This decrease is caused by a greater compliance of the brushes in the boundary region as against the zones that are more remote from the edges. An increase in rigidity or cross-section of the brushes in order to avoid this effect leads at the same time to an insufficient correction

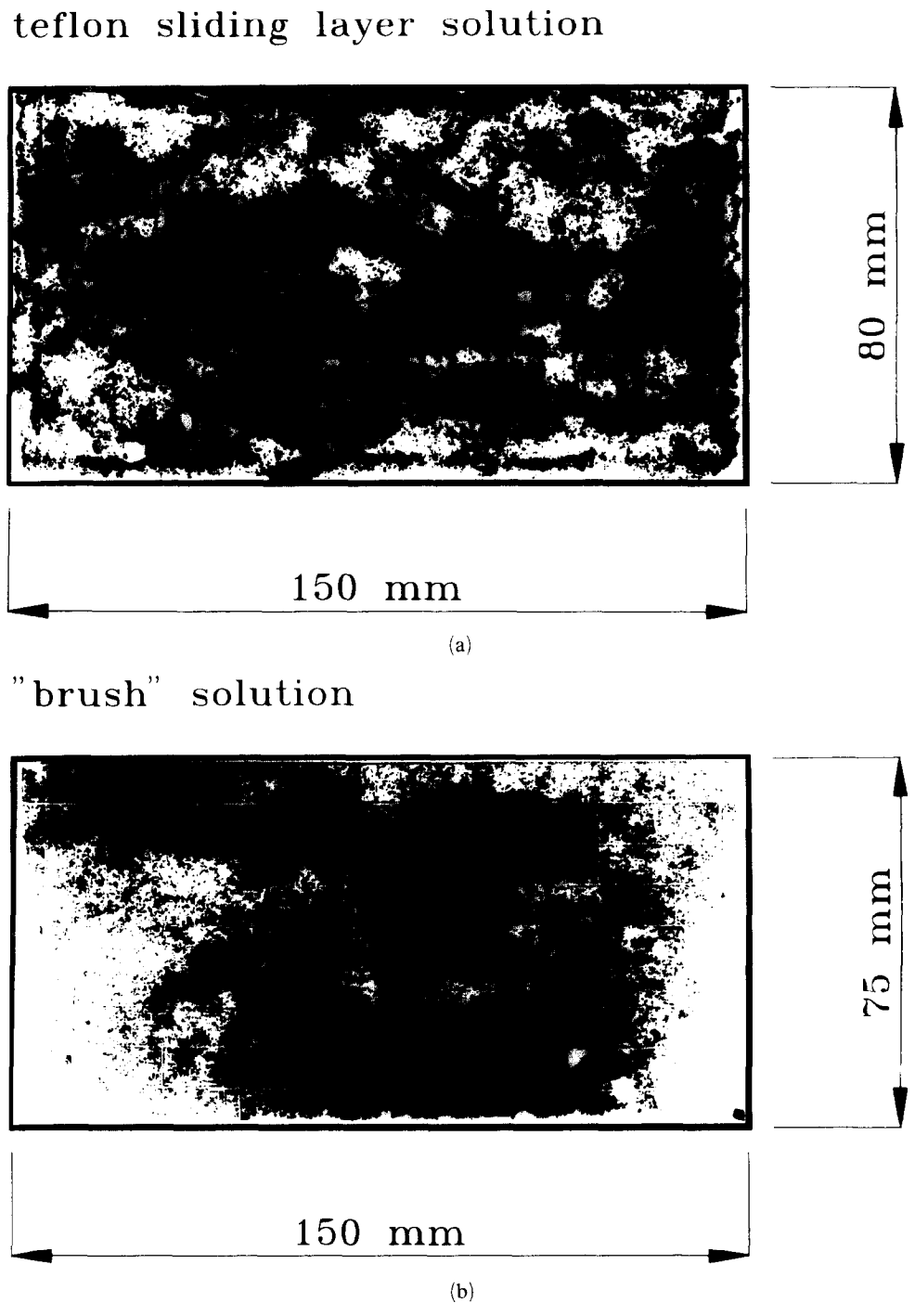

Fig. 5. Pressure measurement foils tests: (a) at the bottom between lower beams and the specimen with the Teflon sliding layer solution; (b) at the bottom between lower beams and the specimen with the 'brush' solution.

of the lateral expansion or transverse strain, respectively, of the two materials.

2.3.3 Series 3: Teflon slabs

Another solution of this problem is offered by the use of Teflon sliding layers (Fig. 3(a)) that are inserted between the ground platens and the contacting surfaces of the concrete specimen. At the bottom the Teflon sliding layers are inserted between the above-mentioned thin plate and the specimen.

The correction of the transverse strain is sufficient if the friction coefficient between steel and concrete parts is as low as possible, due to suitable measures, as described in detail in Ref. 1. Thus, a good grease lubrication is not sufficient (the friction coefficient amounts to approximately 0·3). When using Teflon foils, the friction coefficient is

reduced to approximately 0·02–0·03.[26] According to an estimate, this value is sufficient for a satisfactory correction of the transverse strain for the specimen sizes used in this study. A drop of the compressive stress in the boundary areas, as observed with the 'brush solution', could not be observed here (Fig. 5(a)).

The slipping-off of the load transmission slabs on the teflon foil due to the splitting force active horizontally (this is relevant, in particular, with low σ_1-values) was prevented by increasing the friction between steel and Teflon foil by two grooves that were milled-in about 0·5 mm (5×10^{-4} m) deep immediately close to the starter notch and parallel to the same. This measure does not influence the correction of the transverse strain and has proved to be a sufficient solution for the tests that were carried out, since such a slipping-off has not occurred in one single case.

2.3.4 Series 4: cardboard slabs

This test series is similar to Series 3, however, cardboard slabs with a thickness of approximately 3 mm (3×10^{-3} m) are inserted instead of the Teflon sliding layers.

2.3.5 Results of Test Series 1–4

The same concrete quality was used for all four test series, with a compressive strength f_C of 25 N mm^{-2} (2·5 10^7 Pa), after 28 days of storage in a water bath, with a natural gravel (maximum grain size 16 mm ($1{\cdot}6 \times 10^{-3}$ m)). Since this is the same concrete mixture that was used for the investigation in Section 3, further details can be seen from Table 1. The specimens had the following dimensions: $W \times L \times H = 0{\cdot}15 \times 0{\cdot}15 \times 0{\cdot}13$ m. All specimens were investigated at the same compressive loading stage $\sigma_1/f_C = 50\%$. A minimum of four and a maximum of seven specimens were tested per series. The testing was carried out after 30 days of storage in a water bath.

Table 1. Properties of concrete with natural gravel

Maximum size aggregate (mm)	16
Types of aggregates	Rounded limestone and graywacke
Sand 0–1 mm (kg m^{-3})	404 (20%)
Sand 1–4 mm (kg m^{-3})	404 (20%)
Coarse aggregate 4–8 mm (kg m^{-3})	606 (30%)
Coarse aggregate 8–16 mm (kg m^{-3})	606 (30%)
Water content (kg m^{-3})	173
Cement content (kg m^{-3})	240
Water–cement ratio	0·72
Density (kg m^{-3})	2430
Young's modulus (N mm^{-2})	approx. 30·000

Test series	*NG(wet)*	*NG(dry)*
Age of the specimens when testing (days)	31	30
Compressive cube strength f_c 28 days (N mm^{-2})	24·8	26·2
Flexural tensile strength f_{ft} 28 days (N mm^{-2}) Three-point bending beams (12 × 12 × 36)	5·55	5·90
Water storage (days)	31	7
Number of specimens	24	24

The test data are compiled in Figs 6(a) and (b). The dependence of the specific fracture energy G_f (see Section 3) is shown for the four methods in Fig. 6(a). A considerable increase in specific fracture energy can be observed from Series 4 ($G_f = 86{\cdot}1$ N m^{-1}) via Series 3 ($G_f = 87{\cdot}1$ N m^{-1}) and Series 2 ($G_f = 107{\cdot}4$ N m^{-1}) to Series 1 ($G_f = 148$ N m^{-1}). The nominal notch tensile strength σ_{2max} shows the same tendency, however, with a somewhat smaller slope of the curve (calculated from the maximum value of the load displacement curve; see Section 3) in Fig. 6(b). These experimental results demonstrate clearly that different methods for the correction of the transverse strain can influence the biaxial fracture behaviour considerably. Therefore, we had to judge clearly which of the methods available had to be applied in this study.

Since the methods of Series 1 and 2 supply higher G_f-values and higher notch tensile strengths σ_{2max} compared to the methods of Series 3 and 4, and since the pressure foil measurements display an obvious stress drop in the boundary region of the brushes (Fig. 5(b)), the laminated construction (Series 2) is not employed and neither is the simplest solution (Series 1). For all

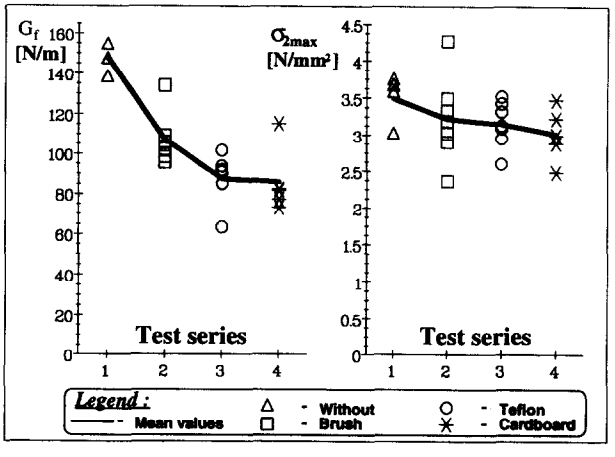

Fig. 6. Results from Test Series 1–4 for the correction of transverse strains: (a) G_f-values for the individual series; (b) σ_{2max}-values for the individual series.

tests that were carried out within the scope of this publication, one method was used exclusively, consisting of a combination of Series 3 and 4. A thick-walled, hard cardboard slab (thickness approximately 3 mm (3×10^{-3} m)) was laid onto the upper and lower surfaces of the specimen, respectively, and a Teflon sliding layer (approximately 0·5 mm (5×10^{-4} m) thick) was inserted between the cardboard and the lower beams or the load transmission slabs, respectively. The cardboard mainly serves as a measure for homogeneous introduction of compression into the specimen, as could be seen from the tests with pressure measurement foils. In addition to that its lateral expansion characteristics, due to its fibrous structure and layer structure, had a positive effect on the correction of the transverse strain. Furthermore, the Teflon–cardboard solution requires less space in the test apparatus and is much cheaper when compared with a costly brush solution.

Table 2. Properties of concrete with crushed gravel

Maximum size aggregate (mm)	16
Types of aggregates	Broken limestone and graywacke
Sand 0–2 mm (kg m^{-3})	707 (35%)
Sand 2–4 mm (kg m^{-3})	303 (15%)
Crushed gravel 4–8 mm (kg m^{-3})	505 (25%)
Crushed gravel 8–11 mm (kg m^{-3})	303 (15%)
Crushed gravel 11–16 mm (kg m^{-3})	202 (10%)
Water content (kg m^{-3})	173
Cement content (kg m^{-3})	240
Water–cement ratio	0·72
Density (kg m^{-3})	2430
Young's modulus (N mm^{-2})	approx. 30·000

Test series	*CG(wet)*	*CG(dry)*
Age of the specimens when testing (days)	31	30
Compressive cube strength f_c 28 days (N mm^{-2})	25·5	26·9
Flexural tensile strength f_{ft} 28 days (N mm^{-2}) Three-point bending beams ($12 \times 12 \times 36$)	5·60	5·85
Water storage (days)	31	7
Number of specimens	22	24

3 INFLUENCE OF GRAIN SHAPE ON BIAXIAL FRACTURE BEHAVIOUR

The objective of this experimental study is to examine the biaxial fracture behaviour of concrete with natural gravel (NG) and crushed gravel (CG), as well as under different storage conditions (dry and wet) for the specimens.

3.1 Material, specimen preparation, measurement procedure and evaluation

The specimens for the biaxial tests (Fig. 1) as well as for the uniaxial tests (Fig. 2) are rectangular blocks, with a base of 0·15 × 0·15 m, a ligament height of 0·11 m and a starter notch depth of 0·02 m. The form of the specimens for biaxial tests is distinguished from the form for uniaxial tests only by the fact that the former has no groove at the upper end of the specimen.

The specimens were cut out of cast blocks with a length of 0·64 m, so that the casting orientation was at a right angle to the direction of compressive loading σ_1. The starter notch was sawn into the specimen by means of a rock cutting saw with a 4×10^{-3} m thick blade. The following four test series were carried out:

Series of measurements with 'wet storage' (storage in water bath):

- Natural gravel, wet — NG(wet);
- Crushed gravel, wet — CG(wet).

With both series the specimens were stored in a water bath for 28 days after the concreting until the test and were tested when still wet.

Series of measurements with 'dry storage':

- Natural gravel, dry — NG(dry)
- Crushed gravel, dry — CG(dry)

With both series the specimens were first stored in a water bath for seven days, then exposed to natural air humidity in the laboratories and then tested in this state.

For these test series, those material compositions were selected that are indicated in Table 1, for natural gravel, and Table 2, for crushed gravel. The mechanical characteristics of the materials are compiled in Tables 1 and 2.

The testing was carried out in a mechanical testing machine (Schenck, RSA 100 type) with a load capacity of 100 kN and a rigidity of 8×10^{-7} m kN^{-1}. Figure 7 gives a survey of the experimental set-up. An elevating frame (Fig. 7, No. 5) that was applied in the centre of the travelling cross-head of the testing machine makes the positioning of the specimen in this loading device easier, since both loading frames are connected to the elevating frame and are clamped to it by appropriate displacement settings so that only the specimens with a previously mounted CMOD-device have to be replaced. With these appropriate displacement settings the two frames can be

arranged in the same symmetric position relative to the starter notch for each test. They are removed if the desired compression level σ_1/f_C (σ_1 = compressive stress, f_C = compressive strength of the material) is achieved. After the specimen has been subjected to compressive loading, the cross-head with the elevating frame travels to the linear support, so that the specimen with the loading unit sits on the same and is raised from the elevating frame. The two frames with the hydraulic cylinders have no mechanical contact with each other or with other parts of the overall construction, apart from, of course, the specimen itself. The CMOD-mounting with the two mounted LVDTs (see Fig. 3(b)) also has no mechanical contact with the rest of the experimental set-up, apart from the specimen, as recommended.[17]

The load cell, the wedge, the starter notch and the theoretical fracture surface, as well as the linear support form one plane, which guarantees that the force flows directly without any detours and, thus, that there is no loss in rigidity in the loading device. Therefore, an unstable crack growth could not be observed with any of the tests carried out within the scope of these investigations.

The cross-head speed amounted to 0·5 mm min^{-1} (5×10^{-4} m min^{-1}) with all investigations and remained constant during the testing. Thus, the loading rate corresponded approximately to the RILEM recommendation.[14] The recording of the measuring results was carried out with a state-of-the-art data acquisition system (DIA/DAGO). With the DIA evaluation programme the following parameters were determined automatically for each measurement.

- maximum splitting force F_H
- notch tensile strength σ_{2max} (nominal value)
- specific fracture energy G_f

In order to characterise the fracture behaviour, the specific fracture energy G_f was used as a basic fracture parameter.

The G_f-value is determined by the mean value curve that results from the arithmetic mean of the two load–displacement curves (F_H-$CMOD_1$ and F_H-$CMOD_2$) and results in:

$G_f = W/A_{Lig}$	G_f-value (in N m^{-1})
W	area under the load–displacement (CMOD) curve
$A_{Lig} = B_{Lig} \cdot H_{Lig}$	area of the plane projection of the ligament area

This definition is taken from the RILEM draft recommendation[14] and has been adapted for the wedge splitting test. The G_f-value is equal to the

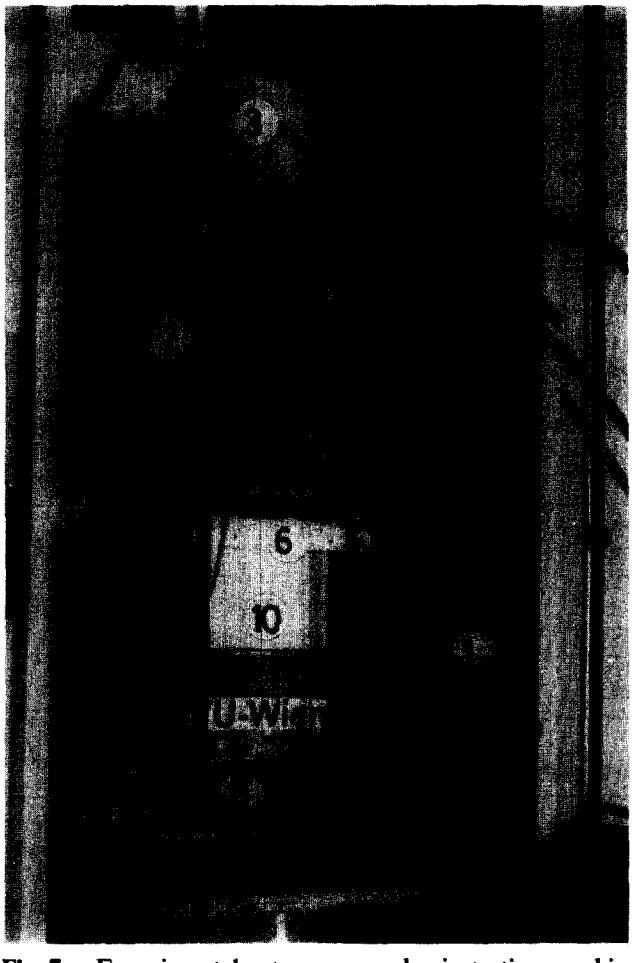

Fig. 7. Experimental set-up — mechanic testing machine with integrated biaxial fracture testing device: (1) testing machine, (2) loading frame, (3) load cell, (4) elongation to the wedge, (5) elevating frame, (6) CMOD-device, (7) LVDT gauge, (8) linear support, (9) hydraulic cylinders, (10) specimen.

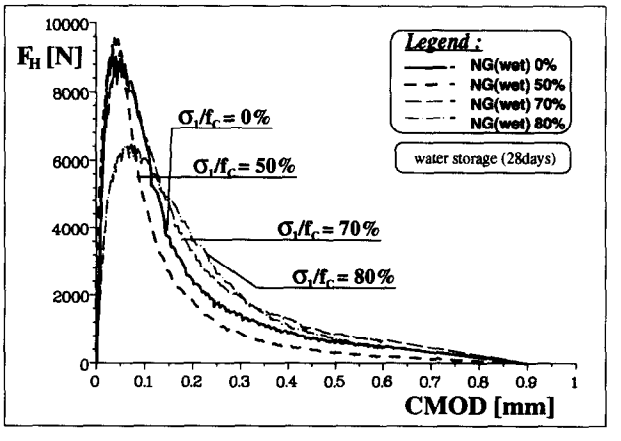

Fig. 8. Typical load–displacement curves from the NG(wet) test series (natural gravel water stored for 28 days) with different loading stages σ_1/f_C.

critical crack driving force G_{Ic}, according to Irwin,[27] only for very brittle materials (with ideal linear elastic behaviour).

A nominal *notch tensile strength* σ_{2max} was calculated as follows:

$$\sigma_{2max} = \frac{M}{W_{Lig}} + \frac{F_{Hmax}}{A_{Lig}}$$

$$M = y.F_{Hmax}$$

$$W_{Lig} = \frac{B_{Lig}.H_{Lig}^2}{6}$$

where M is the maximum moment, y being the distance of the axis of force application to the centre of the ligament area and W_{Lig} is the maximum moment of resistance referred to the notch root.

3.2 Results

In Fig. 8 typical load–displacement curves of the NG(wet) series are shown with σ_1-loadings of 0, 50, 70 and 80% f_c. With increasing σ_1-loading the maximum of the curve decreases. The decreasing branch of the curve — the post-peak behaviour — after the maximum is, however, decreasing less with increasing σ_1-loading, i.e. more energy is consumed in this range. In general the trend described can be observed with all measure test series. The course of the measured load–deformation curves does not show any discontinuous parts of the curve that would indicate an instable crack propagation.

3.2.1 Influence of grain shape and storage conditions

Test series 'wet storage'. Tables 3 and 4 contain the mean measurement results of the number of tests indicated in the respective last column for the Test Series NG(wet) and CG(wet) of the Test Series 'wet storage'.

This most important and most interesting result is represented graphically in Figs 9(a) and 9(b). The curves of the mean values of the measured G_f-values (Fig. 9(a)) and the curves of the normalized G_f/G_{f0} values (G_{f0} = specific fracture energy with uniaxial loading) (Fig. 9(b)) are plotted versus the compressive loads σ_1/f_C. In Fig. 10 the values for the notch tensile strength σ_{2max} are plotted versus the compressive loads σ_1/f_C. Figures 9(a) and 9(b) are characteristic for biaxial loading of cement-bound materials[13,25] and shall therefore be commented on in greater detail.

With an increasing load σ_1/f_C you can first of all observe a drop of the G_f-value to a minimum. With a further increase of σ_1/f_c, a rise of the G_f-value up to a maximum at approximately σ_1/f_C = 80% can be registered. The following scenario

Table 3. Mean values of the results of the test series for natural gravel (water storage 28 days) (NG(wet))

Norm. compressive stress σ_1/f_C *(%)*	*Notched tensile strength* σ_{2max} *(N mm^{-2})*	*Spec. fracture energy* G_f *(N m^{-1})*	*Norm. spec. fracture energy* G_f/G_{f0} *(%)*	*Number of specimens (n)*
0	3·54	113·8	100·0	5
15	3·33	78·1	68·6	2
30	2·98	78·0	68·5	3
40	3·64	94·2	82·8	3
50	3·30	89·2	86·8	5
70	3·20	111·2	97·7	3
80	2·62	116·2	102·4	3

Table 4. Mean values of the results of the test series for crushed gravel (water storage 28 days) (CG(wet))

Norm. compressive stress σ_1/f_C *(%)*	*Notched tensile strength* σ_{2max} *(N mm^{-2})*	*Spec. fracture energy* G_f *(N m^{-1})*	*Norm. spec. fracture energy* G_f/G_{f0} *(%)*	*Number of specimens (n)*
0	3·64	105·4	100·0	3
20	3·50	87·8	83·3	3
30	4·00	106·0	100·7	3
40	3·83	100·4	95·2	3
50	3·64	98·4	93·3	3
70	3·67	111·5	105·8	3
80	2·49	119·4	113·3	3

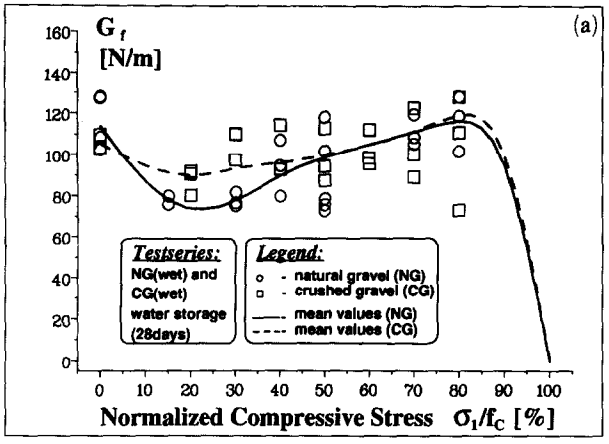

Fig. 9. Influence of compressive loading σ_1 on the specific fracture energy G_f for natural gravel (NG) and crushed gravel (CG) after wet storage over 28 days: (a) G_f-values vs loads σ_1/f_C; (b) normalised G_f/G_{f0}-values vs loads σ_1/f_C.

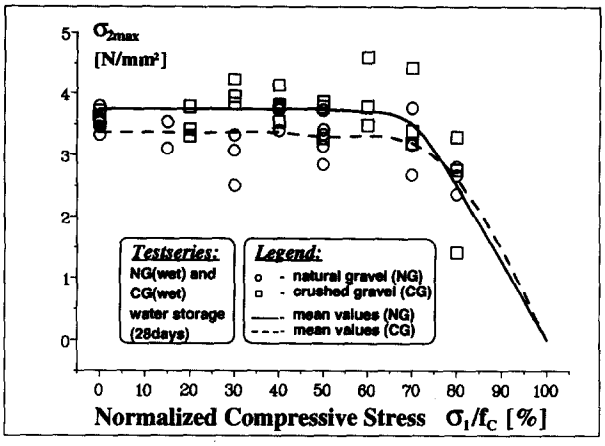

Fig. 10. Failure envelope of notch tensile strength σ_{2max} against the compressive loading σ_1 for natural and crushed gravel after water storage for at least 28 days.

results: for the test series NG(wet) the G_f-value falls (see Figs 9(a) and 9(b), full line) from $G_{f0} = 113{\cdot}8$ N m^{-1} ($G_f/G_{f0} = 100\%$) to 78·0 N m^{-1} ($G_f/G_{f0} = 68{\cdot}5\%$) with a load $\sigma_1/f_c = 30\%$ (minimum at $\sigma_1/f_c \cong 20\%$) and then increases continuously up to 116·2 N m^{-1} for a compressive load $\sigma_1/f_C = 80\%$ ($G_f/G_{f0} = 102{\cdot}4\%$).

This can be compared with the CG(wet) series, where the G_f-value (see Figs 9(a) and (b), dash line) falls from $G_{f0} = 105{\cdot}4$ N m^{-1} ($G_f/G_{f0} = 100\%$) to 87·8 N m^{-1} ($G_f/G_{f0} = 83{\cdot}3\%$) with a compressive load $\sigma_1/f_C = 20\%$ (minimum) and then increases continuously up to 119·4 N m^{-1} for a compressive load $\sigma_1/f_C = 80\%$ ($G_f/G_{f0} = 113{\cdot}3\%$).

The different biaxial fracture behaviour is in the first place due to the different grain shapes of the aggregate used. This topic still requires detailed discussion.

In analogy with the classical pre-peak behaviour in the tension–compression range, the curves of the two test series NG(wet) and CG(wet) (see Fig. 10) with regard to the notch tensile strength σ_{2max} are plotted versus the loads σ_1/f_C. They have the well-known biaxial envelope shape. This shape is characterised by constant values of σ_{2max} until a compressive load of approximately $\sigma_1/f_C = 75\%$, as was also found by Zielinsky[11] and Kotsovos and Newman.[28] In contrast to that a continuous decrease of the tension stress with increasing compressive stress was observed on unnotched specimens in older studies.[1-4] To determine if this behaviour is due to the use of notched or unnotched specimens or to the formation of several fracture process zones, respectively, will require further investigation by experimental and theoretical studies and will not be treated here any more.

Test series 'dry storage'. In analogy with the results of the 'wet storage' series, the measured results for the Test Series 'dry storage' for NG(dry) and CG(dry) are compiled in Tables 5 and 6.

The curves for the G_f mean values, as well as for the normalised G_f/G_{f0} mean values with increasing compressive loads σ_1/f_C (Figs 11(a) and 11(b)), show essentially the same decreasing and increasing behaviour as the series of measurements for 'wet storage'. An important difference to Figs 9(a) and 9(b) can be seen from the position of the minimum values of the curves.

Whereas the minimum for the NG(wet) series ($G_f = 78$ N m^{-1}, $G_f/G_{f0} = 68{\cdot}5\%$) is at approximately $\sigma_1/f_C = 20\%$, the minimum value for NG(dry) ($G_f = 86{\cdot}6$ N m^{-1}, $G_f/G_{f0} = 63{\cdot}4\%$) is at approximately $\sigma_1/f_C = 35\%$. For the CG(wet) series ($G_f = 87{\cdot}8$ N m^{-1}, $G_f/G_{f0} = 83{\cdot}3\%$) the minimum is at approximately $\sigma_1/f_C = 20\%$, whereas for CG(dry) ($G_f = 84{\cdot}3$ N m^{-1}, $G_f/G_{f0} = 63{\cdot}5\%$) it is at approximately $\sigma_1/f_C = 40\%$.

Table 5. Mean values of the results of the test series for natural gravel (water storage seven days) (NG(dry))

Norm. compressive stress σ_1/f_C *(%)*	*Notched tensile strength* σ_{2max} *(N mm^{-2})*	*Spec. fracture energy* G_f *(N m^{-1})*	*Norm. spec. fracture energy* G_f/G_{f0} *(%)*	*Number of specimens (n)*
0	3·38	136·5	100·0	4
20	2·89	93·1	68·1	3
35	2·78	86·6	63·4	3
50	3·17	107·6	78·8	3
60	3·00	101·6	74·4	3
70	3·04	114·5	83·9	3
80	2·43	91·8	67·3	3

Table 6. Mean values of the results of the test series for crushed gravel (water storage seven days) (CG(dry))

Norm. compressive stress σ_1/f_C *(%)*	*Notched tensile strength* σ_{2max} *(N mm^{-2})*	*Spec. fracture energy* G_f *(N m^{-1})*	*Norm. spec. fracture energy* G_f/G_{f0} *(%)*	*Number of specimens (n)*
0	3·67	132·8	100·0	5
20	3·46	97·7	73·6	3
30	3·43	88·3	66·5	3
40	3·15	84·3	63·5	3
50	3·32	101·8	76·7	3
60	4·11	129·7	97·7	3
70	3·33	111·0	83·6	3

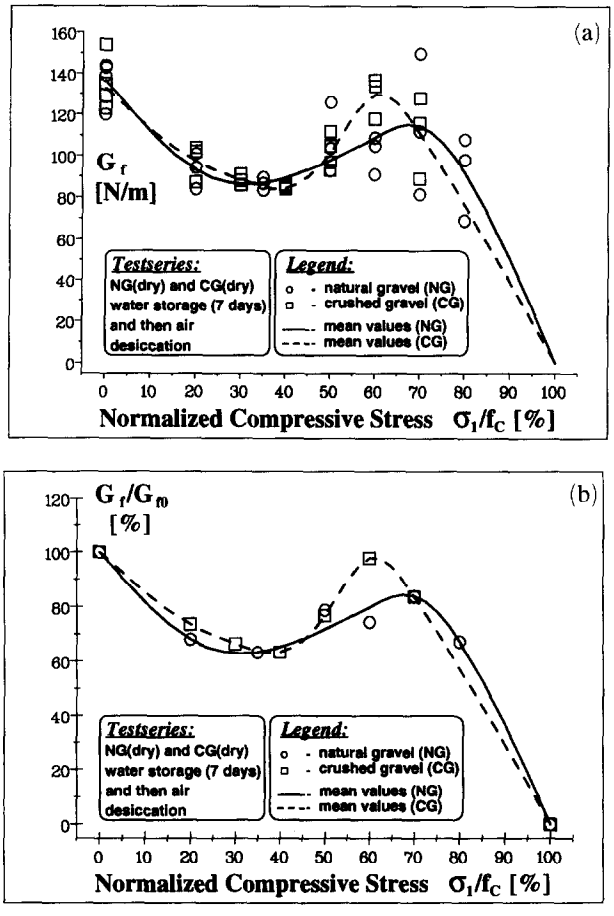

Fig. 11. Influence of the compressive loading σ_1 on the specific fracture energy G_f for natural gravel (NG) and crushed gravel (CG) after wet storage for seven days and subsequent dry storage: (a) individual G_f-values vs loads σ_1/f_C; (b) normalised G_f/G_{f0}-values vs loads σ_1/f_C.

The difference of the reduction of G_f/G_{f0} for their minimum values of the two series of measurements (wet/dry) is much larger for CG ($\cong$ 20%) than for NG ($\cong$ 5%).

Whereas the minimum values for 'dry storage' are shifted towards larger σ_1/f_C values, a reverse tendency can be observed with the maximum values for 'dry storage' (shift towards lower σ_1/f_C values). The following maximum mean values were determined:

- NG(wet): $\sigma_1/f_C = 80\%$, $G_f = 116{\cdot}2$ N m^{-1}, $G_f/G_{f0} = 102{\cdot}4\%$.
- NG(dry): $\sigma_1/f_C = 70\%$, $G_f = 114{\cdot}5$ N m^{-1}, $G_f/G_{f0} = 83{\cdot}9\%$.
- CG(wet): $\sigma_1/f_C = 80\%$, $G_f = 119{\cdot}4$ N m^{-1}, $G_f/G_{f0} = 113{\cdot}3\%$.
- CG(dry): $\sigma_1/f_C = 60\%$, $G_f = 129{\cdot}7$ N m^{-1}, $G_f/G_{f0} = 97{\cdot}7\%$.

The biaxial failure envelopes (Fig. 12) for the NG(dry) and CG(dry) series, however, show the same constant curve as those of Fig. 10 up to approximately $\sigma_1/f_C = 75\%$, however, the average notch tensile strengths σ_{2max} are lower for the two series of measurements of 'dry storage', as can be seen from the following:

- NG(wet): σ_{2max}(average) $\cong$ 3·3 N mm^{-2}.
- NG(dry): σ_{2max}(average) $\cong$ 3·0 N mm^{-2}.
- CG(wet): σ_{2max}(average) $\cong$ 3·8 N mm^{-2}.
- CG(dry): σ_{2max}(average) $\cong$ 3·3 N mm^{-2}.

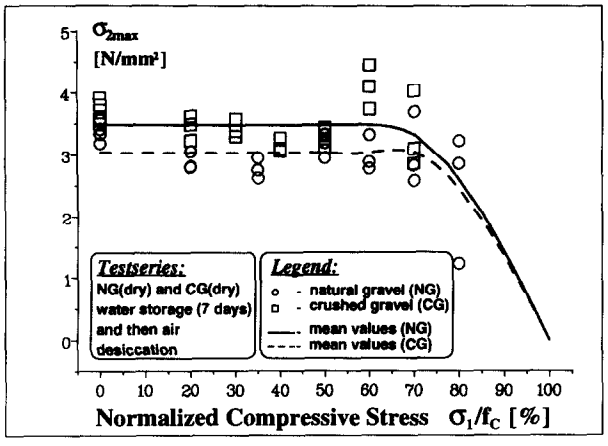

Fig. 12. Failure envelope of notch tensile strength σ_{2max} *vs* the compressive loading σ_1 for natural gravel (NG) and crushed gravel (CG) after wet storage for seven days and subsequent dry storage.

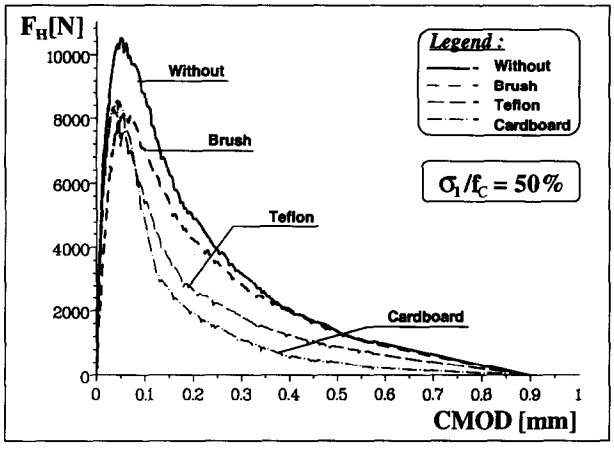

Fig. 13. Typical load (F_H)-displacement (CMOD) curves from Series 1–4 for the correction of transverse strain.

4 DISCUSSION

4.1 Correction of transverse strain

A restraint of transverse strain with biaxial material testing can obscure the proper interpretation of the measured material characteristics. Thus, the fracture characteristics may be in error in case of an insufficient correction of the transverse strain, as can be demonstrated by means of the measured load–displacement curves (they contain all information necessary for a sufficient characterisation of the fracture behaviour).

From Test Series 1–4 (Section 2.3) one typical load–displacement curve each was selected and was compiled in Fig. 13. These curves were measured on the same material, with the same form of specimen, the same testing method, and only with different methods for the correction of the transverse strain. From the F_H–CMOD curves we can see immediately how far different methods for the correction of transverse strain influence the fracture behaviour. Height of the peak as well as fracture energy (area under the curve) are clearly different for the different measures (see also Figs 6(a) and (b)). The Teflon and cardboard methods show a steep drop in Fig. 13 against the two other curves in the post-peak range of the load–displacement curves. Therefore, the brush solution and 'without' present a more ductile fracture behaviour of the material as against the two other solutions. The increase in this 'pseudo'-ductility with an increasing limitation of lateral deformation is exclusively an expression of the methods used for the correction of the transverse strain, and thus it is no real material characteristic.

Different solutions for the correction of the transverse strain have already been the subject of scientific investigations in literature several times. For example, Kupfer *et al.*[1] investigated the influence of different methods on the mechanical properties of unnotched concrete specimens under biaxial loading. The measures applied were high boundary restraint measures, such as steel plate on concrete, and low boundary restraint measures, such as laminated constructions. Further examples are the papers by Vonk and co-authors[26,29,30] that have appeared only recently. They report experimental studies of the softening behaviour of unnotched concrete samples with uniaxial compression loading, under different boundary conditions referring to the correction of transverse strain. With regard to boundary conditions that limit the transverse strain, both high-boundary restraint measures (dry steel platens) and low-boundary restraint measures (short and long brushes as well as Teflon platens with greased steel platens) were used in Refs 26, 29 and 30.

If we compare the results found in Refs 1, 26, 29 and 30, and in this paper, we can generally find a good correspondence. The correction of transverse strain is improved by the measures mentioned below in the following sequence: dry platen; short brushes; long brushes; and finally, a Teflon sliding layer and a cardboard layer.

When selecting a method for the correction of the transverse strain, the function of the testing method also has to be considered as a second aspect, as will be shown below:

- With the biaxial fracture tests — as carried out in this paper — a constant compressive

stress is applied to the specimen, and thus a corresponding constant friction stress occurs when using Teflon sliding layers and cardboard slabs, and a constant shear stress occurs when using brushes, in addition to this stress. Both of them remain constant during the entire curve of the experiment. For this loading, the material is loaded only in the pre-peak range. Its lateral deformation is mostly low when compared to a post-peak loading.

- With the uniaxial compression tests[26] friction stress increases with rising normal stress and reaches a maximum under the peak stress, then it decreases with the post-peak softening curve. In contrast to this the shear stress is an increasing function with increasing lateral deformation, also in the softening range.[31] Due to the fact that the transverse strains have different values in the pre-peak and post-peak ranges, an insufficient correction of the transverse strain in the pre-peak range is much less noticeable than it is in the post-peak range.

In case a uniaxial compression test is carried out, e.g. the brush solution with increasing lateral deformation shows a growing bend of the brushes and, thus, also an increase in shear stress, which on its part causes a reduction of the correction of transverse strain. With the Teflon–cardboard solution, on the other hand, the friction only depends on the compressive stresses and not on lateral deformation. With biaxial fracture tests this different behaviour does not have such a strong effect, since lateral deformation may become rather small. Thus, only if seen *exclusively* from the point of view of the correction of transverse strain with biaxial fracture tests, both the Teflon–cardboard method and the brush method can be applied, whereas with uniaxial compression testing the Teflon–cardboard method is absolutely preferable to the brushes method. This is due to the large lateral elongation (in particular in the post-peak range), as has been justified and carried out in Ref. 26. However, also with the biaxial fracture tests the Teflon–cardboard method is preferable to the brush method, since the former guarantees a more homogeneous force initiation in the specimen (see Figs 4(a) and (b)).

A third aspect is that unnotched and notched specimens play a role in the selection of the method for the correction of transverse strain. The reason for this is that the fracture process zone which determines the fracture behaviour only begins in the notch root, and, thus, is at a certain distance from the introduction of compression. Possibly occurring inhomogeneous stress characteristics caused by different corrections of transverse strain, or also by compressive stresses applied irregularly by the loading unit, can be diminished at least partly by the notched upper end of the specimen itself. Thus, biaxial fracture tests — as carried out in this study — are much less sensitive to under correction of the transverse strain than, e.g., uniaxial compression tests.

We have to add that none of the investigated methods for the correction of transverse strain can be classified as being the 'ideal method'. The ideal correction would be realised by a device that completely follows the lateral deformation of the specimen during the application of compression and, in addition to this, also allows a homogeneous and constant force initiation in the specimen.

4.2 Influence of grain shape and storage conditions

Material characteristics, size and shape of the fracture process zone (FPZ) that is being formed, as well as the degree of pre-damage of the material that is comprised by the FPZ, basically determines the fracture energy and, thus, also the fracture behaviour of the material. The energy dissipation processes that proceed around the crack tip can be split into basically two different mechanisms:[32]

- 'microcracking' — microcracking in the FPZ *before the crack tip*
- 'bridging' — friction and interlock between matrix and aggregates *behind the crack tip*

With the bridging mechanism, forces can be transmitted from aggregates that bridge the two crack flanks behind the crack tip.

By means of these two main mechanisms and in combination with a modified phenomenological model according to Ref. 13, the influences on the biaxial fracture behaviour of concrete that were found experimentally are analysed and discussed. The model is represented in Fig. 14 and shows the schematic dependence of the normalised specific fracture energy G_f/G_{f0} on the normalised compressive stress σ_1/f_C. This curve is subdivided into four typical loading ranges (a–d) and will be treated accordingly below.

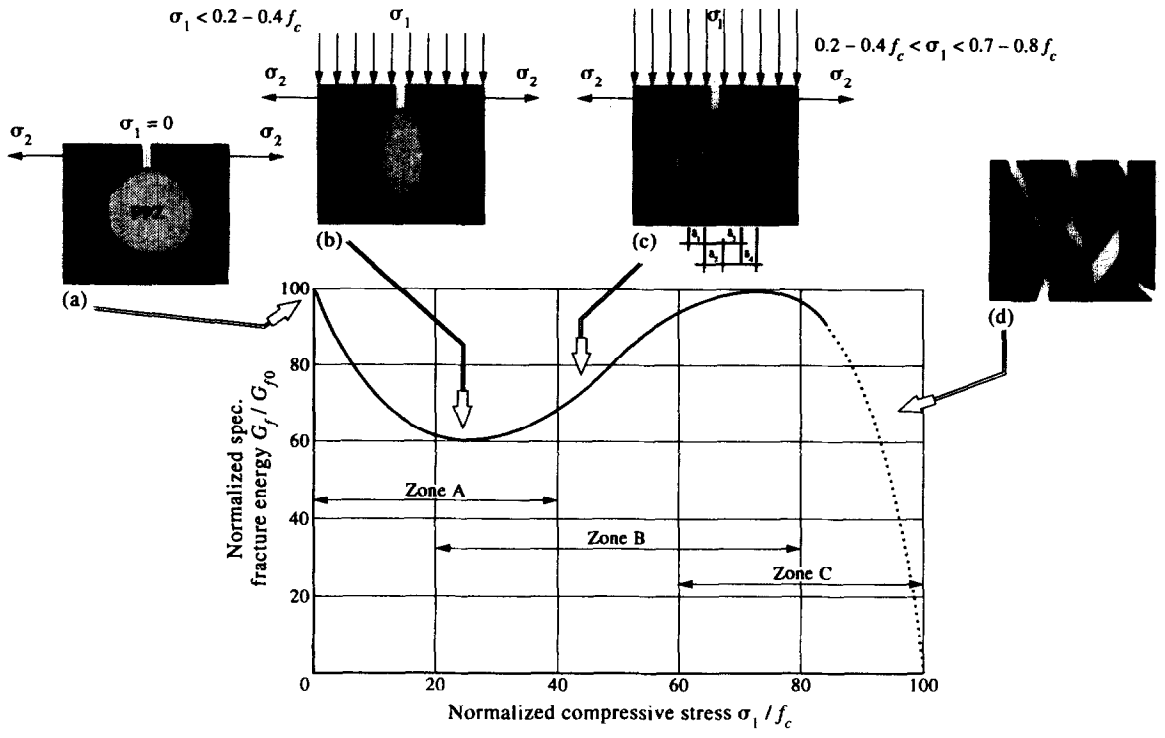

Fig. 14. Fracture model for the various stages of σ_1 loading (the values approaching $\sigma_1/f_C = 1$ are extrapolated and characterised by a dashed line): (a) $\sigma_1 = 0$, uninfluenced formation of the fracture process zone (FPZ); (b) constraint of FPZ due to σ_1; (c) increase in fracture energy friction in the microcracked material and possible multiple macrocracking; (d) total failure.

4.2.1 Range a: $\sigma_1 = 0$ (Fig. 14(a))

The FPZ develops in an unrestricted way. The distribution of fracture energy into microcracking and bridging mechanisms also remains uninfluenced. Both for the series of measurements NG(wet) and CG(wet) the G_{f0} values in the magnitude of 100 N m^{-1} are achieved, whereas for NG(dry) and CG(dry) G_{f0} values of $\cong$ 135 N m^{-1} are measured.

This difference of the G_{f0} values ($\cong$ 25 N m^{-1}) is caused by the different friction conditions in the interface aggregate–matrix. As described in Ref. 33, the presence of water reduces the internal friction coefficient. For the series of measurements of 'wet storage' the entire specimen is moistened, which causes a kind of 'lubrication' in the interface aggregate–matrix, whereas for the series of measurements of 'dry storage' an increased (dry) friction occurs between aggregate and matrix. This influences above all the energy consumption of the bridging component, since less energy is dissipated with 'wet storage' than with 'dry storage', due to the reduced friction.

4.2.2 Range b: $\sigma_1 < 0{\cdot}3 f_c$ (elastic range) (Fig. 14(b) Zone A)

The biaxial state of stress also influences the FPZ by creating a thinner and also smaller FPZ. In the horizontal direction the formation of microcracks is suppresed, or the existing ones are closed, respectively, whereas in the vertical direction microcracks are initiated and opened. This leads to a straightening of the crack path, as a semi-quantitative analysis in Ref. 25 has shown. The decrease in fracture energy is due to the smaller FPZ and to a reduction of the main crack branching.

In Zone A the 'microcracking' component for both forms of aggregates decreases, whereas the 'bridging' component for natural gravel remains equal to the situation with uniaxial loading, since the inner compound is still intact and since there is no change in the friction and interlocking ratios in microstructure (aggregate and matrix compound).

The volume/surface ratio is larger for crushed gravels than for natural gravels. Thus, a larger compound area results for all crushed gravels, and also a larger friction surface between matrix and aggregates than for natural gravels with the same concrete volume. The resulting stronger compound for crushed gravel in the interlock behind the crack tip causes a higher bridging component than for natural gravel, even with smaller loadings. Furthermore, the rough fracture surface of the aggregate contributes considerably to the higher

energy dissipation (in contrast to natural gravel) when the crushed gravels are pulled out from the interlock. However, this increase in the bridging component for crushed gravel does not compensate for the decrease in the microcracking component, which results in a smaller decrease in fracture energy for crushed gravel as compared to natural gravel.

For the two series NG(dry) and CG(dry) of 'dry storage' the larger drop of the fracture energy against the two series NG(wet) and CG(wet) of 'wet storage' (compare Figs 9(a) and 9(b) and 11(a) and 11(b)) can be explained by impeding the process of setting. During the hardening of the concrete, hydrous compounds are formed; the so-called hydrate phases. The crystalline structure, an interlocked mineral structure of crypto-crystalline hydrates, is of decisive importance both for the global and for the local characteristics of the concrete texture. The interrupted water supply stops the crystallisation also at the interface aggregate–matrix, which finally results in a weaker compound. Under compressive loading even the crystallites that are weakly connected and the more weakly bound aggregates can now rearrange themselves more easily. By means of this process the stress concentrations are diminished more easily, thus, creating a slenderer FPZ when compared with the series of 'wet storage'. With higher loading stages ($\sigma_1 > 0{\cdot}4\ f_C$) the optimum degree of rearrangement has been reached (minimum values in Figs 11(a) and (b)), and an increase of the aggregate interlock takes effect.

4.2.3 Range c: $0{\cdot}3 f_c > \sigma_1 > 0{\cdot}8 f_c$ (Fig. 14(c) Zone B) (non-linear deformation range)

In general an increase in σ_1-stress leads to an enlargement of vertical microcracks. These are formed increasingly in the entire specimen and are accompanied by an increasing failure of the matrix and the interface between the matrix and the aggregates. Therefore, the aggregates increasingly have to carry the applied σ_1-stress. For both forms of aggregates the friction between aggregate–matrix and aggregate–aggregate or the energy dissipation when extracting from the interlock, respectively (aggregate interlock), is increased drastically behind the crack tip. With increasing σ_1-stress the component of the bridging mechanism increases by a multiple against a further decrease of the microcracking component. All in all this leads to an increase in total fracture energy.

As can be seen from the figures (Figs 9(a) and 11(a)), the scatterings of the measured values with loads $\sigma_1/f_C > 60\%$ increase significantly against lower load levels with both test series. Such a behaviour was also observed by Zielinski[11] with impact tensile compression tests with some specimens for $\sigma_1/f_C > 50\%$. This is explained in Ref. 11 by multiple fracturing behaviour. In Ref. 8 equally wide scatterings are observed with triaxial tests in the tension–compression range for larger loadings $\sigma_1/f_C > 60\%$. Van Mier explains these scatterings in Ref. 8 by multiple microcracking and by the transition of various fracture modes.

In a fractographic study it was clarified whether the reasons found in Refs 8 and 11 for the scattering of the measured values are also applicable to the findings of the work reported here. This study yielded the following result: Fig. 15 shows the main crack and the fracture surfaces of a specimen of the NG(wet) series with a high G_f-value of 131·8 N m^{-1}. In Fig. 15(a) a multiple branched main crack in the ligament area can be seen and

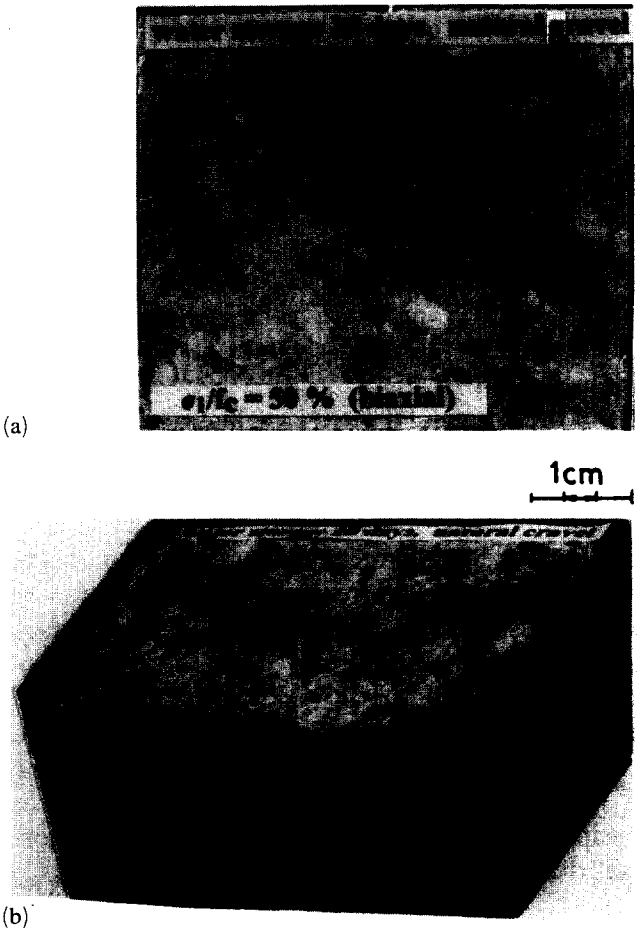

Fig. 15. Fractographic investigation: (a) path of the main crack in a specimen from the NG(wet) series; (b) detail of a fracture surface of a specimen with crack branching and with multiple cracking, respectively.

on the fracture surfaces (Fig. 15(b)) large-area 'flakes' can be discerned that do not stretch over the entire fracture surface or the entire specimen, respectively. These fractographic characteristics can, however, not be observed with specimens of the same series and the same loading stage of σ_1/f C = 50% with lower specific fracture energy (e.g. 89·2 N m^{-1}). The large scatterings of the measured values are therefore unambiguously due to multiple macrocracking and crack branching.

As these considerations have shown, more pronounced crack branching and multiple cracking lead to higher measured G_f-values. Therefore, we have to suppose that the specific fracture energy in Zone B is determined by the (i) bridging component mentioned in the beginning and of (ii) multiple macro-cracking and crack branching. Therefore, these two failure modes have to be taken into consideration in the fracture model for biaxial loading, where multiple macrocracking and microcracking can be observed in the specimen (Fig. 14(c)).

For the test series NG(wet) this loading rate has the same G_f mean values as CG(wet) (Figs 9(a) and 9(b)). The two curves are parallel in the normalised diagram (Fig. 9(b)). An explanation for this curve could be that due to their naturally rounded shape natural gravels can slip off more easily than crushed gravels in the interlock behind the crack tip in the environment of the already damaged matrix (similar to 'ball joints').

The shift of the two maximum values towards lower loads, as well as the higher maximum value for the CG(dry) series (Figs 11(a) and 11(b)) in contrast to the NG(dry) series, cannot be explained on the basis of the investigations that have been carried out so far.

4.2.4 Range d: $\sigma_1 > 0{\cdot}7$–$0{\cdot}8 f_c$ (Fig. 14(d) Zone C)
If the compressive stress σ_1 is increased beyond 0·7 or 0·8 f_C, there is a multiple fracturing of the specimen (see schematic in Fig. 14(d)), the aggregate interlock loses its effect due to the occurring excessive disintegration and enlargement of the compound and this leads to a breakdown and to the disintegration of the microstructure (aggregate and matrix compound) (Zone C in Fig. 14).

It should be mentioned that some energy is dissipated during compressive loading of the specimen ($\sigma_1/f_C > 0\%$) which leads to more or less damage of the microstructure (e.g. formation or elongation of microcracks). If, however, the ratio (σ_1/f_C) approaches 1, the fracture energy G_f will become zero. In this case, the energy needed for disintegration and fracturing of the specimen is completely supplied by the compressive stress σ_1.

If we consider the measured load–displacement curve in Fig. 8 in connection with this model, the following picture results.

The lowering of the curve peak with higher σ_1/f_C values ($\sigma_1/f_C > 60\%$) against lower values can be explained by the fact that a high compression loading causes a pronounced microcraking in the ligament area or a pre-damage, respectively, and that, thus, a crack initiation occurs even with low splitting force values F_H.

The different decrease in the post-peak range of the measured curves can be traced to the effect of the increased 'bridging' effect with high σ_1-stresses. The 'apparent' ductility at the end of the curve seems to follow the mechanism of the frictional resistance mainly by simple and multiple cracking with aggregate–aggregate or aggregate–matrix interlocks, respectively, that occur more strongly with high σ_1-stresses.

These preliminary findings require further research. They may, however, be useful for the formulation of damage models, especially for assessing the post-earthquake stability of massive concrete structures.

Finally, it should be mentioned that the authors are aware of the unsolved size-effect problem[34,35] for both uniaxial and biaxial loading. This is to be studied for a range of specimen dimensions on the basis of experience with loading equipment.

5 CONCLUSIONS

By means of a new biaxial wedge splitting equipment the fracture behaviour of concrete with various aggregates (crushed gravels or natural gravels, respectively) after wet storage and dry storage of the specimen was investigated. The following results were found:

(1) The combination of the splitting method according to Tschegg[15,16] with a hydraulic compressive loading unit for the realisation of a biaxial state of stress in a cubic, laterally notched specimen has proved to be a simple testing method that is easy to use and inexpensive. This test apparatus can be integrated into usual testing machines without any particular effort. Due to the high stiffness of the test system a stable crack growth until the complete separation of the specimen can be expected even for brittle materials.

(2) The realisation of a homogeneous and defined state of stress in the specimen is achieved by means of a stiff construction of the loading frames and by arranging several hydraulic cylinders in a row, as an experimental check with pressure measurement foils has shown (Fig. 4).

(3) The influence of various methods for the correction of transverse strain between the steel platens and the concrete sample was investigated experimentally. It was found that the insertion of sliding layers had the least influence on the measured result when they were inserted in the following sequence: steel plates, teflon layer, cardboard slab, concrete specimen. The 'brush solution' that has been most frequently used up to now clearly shows disadvantages against the Teflon–cardboard solution.

(4) With uniaxial loading ($\sigma_1 = 0$) of concrete with a compressive strength of approximately 25 N mm^{-2} and a maximum grain size of 16 mm the following specimen fracture energy values (G_{f0}) were found for wet storage and dry storage of the specimens:

Crushed gravels: CG(wet), 105 N m^{-1}; CG(dry), 133 N m^{-1}.
Natural gravels: NG(wet), 114 N m^{-1}; NG(dry), 136 N m^{-1}.

With increasing σ_1-values the specific fracture energy falls, the drop being at about 40% for NG(wet) and 18% for CG(wet) in reference to the G_{f0} values. The minimum is reached at a biaxial loading of $\sigma_1/f_C = 30\%$ for NG(wet) and at 40% for CG(wet).

With dry storage the drop of the G_f-value for CG(dry) and NG(dry) amounts to about 13%. The minimum is reached at approximately $\sigma_1/f_C = 20\%$ for NG(dry) and at approximately 40% for CG(dry).

With a further increase of the σ_1/f_C value the specific fracture energy increases again and reaches a maximum with σ_1/f_C values of 80% after wet storage and of 60–70% after dry storage. These maximum values for G_f are about 20% higher for the series (NG(wet), CG(wet)) after wet storage than for the series (NG(dry), CG(dry)) after dry storage.

(5) If the nominal notch tensile stress σ_{2max} is plotted versus σ_1/f_C values in analogy to the failure envelopes of classical biaxial investigations, the notch tensile strengths up to $\sigma_1/f_C = 75\%$ remain constant. This behaviour is in accordance with other recent studies.[11,28] For both wet storage and dry storage higher notch tensile strengths (σ_{2max}) are obtained for CG than for NG.

(6) Under biaxial loadings of $\sigma_1/f_C > 50\%$ the scattering of the measured values increases significantly. This increase can be traced to the formation of several macroscopic cracks in the process zone, as can be seen from fractographic investigations.

(7) The decrease and increase of the specific fracture energy under increasing biaxial loading can be explained qualitatively by means of a model. The interaction of energy-dissipating processes before ('microcracking') and after ('bridging') the crack tip that are influenced by biaxial loading generally determine the fracture behaviour of the material.

ACKNOWLEDGEMENTS

We would like to thank Mr A. Pölzl, BPV Lanzendorf, for his expert manufacturing of the specimen. We would also like to thank Mr A. Lahner for the manufacturing production of the biaxial equipment for the splitting test. Dr H. Kreuzer has promoted our work very much by stimulating discussions, for which we would like to thank him. This project was financed by the Fonds zur Förderung der wissenschaftlichen Forschung (Austrian Science Foundation) under the project number P 8885-TEC.

REFERENCES

1. Kupfer, H., Hilsdorf, H. K. & Rüsche, H., Behavior of concrete under biaxial stress. *ACI J.*, (1969) 656–66.
2. Kupfer, H. & Gerstle, K. H., Behavior of concrete under biaxial stresses. *J. of Eng. Mech. Division, ASCE*, **99** (EM4) (1973) 583.
3. Nelissen, L. J. M., Biaxial testing of normal concrete. *HERON*, **18** (1) (1972).
4. Rosenthal, I. & Glucklich, J., Strength of plain concrete under biaxial stress. *ACI J.*, (1970) 903–13.
5. Gerstle, K. H. *et al.*, Behavior of concrete under multiaxial stress states. In *Proc. ASCE*, Vol. 106, No. EM6, December 1980, pp. 1383–404.
6. Kotsovos, M. D. & Newman, J. B., Behavior of concrete under biaxial stress. *ACI J.*, (1977) 443–6.
7. Huang, J. L., Dahai, H. & Nianxiang, X., Behavior of concrete under triaxial compressive–compressive tensile stresses. *ACI Materials J.*, (1991) 181–5.
8. Van Mier, J. G. M., Fracture of concrete under complex stress. *HERON*, **31** (3) (1986).

9. Van Mier, J. G. M., Multiaxial strain softening of concrete, part I: Fracture, part II: Load histories. *Materials and Structures RILEM*, **19** (III) (1986).
10. Weerhejim, J., Concrete under impact tensile loading and lateral compression. PhD thesis. Prins Maurits Laboratory TNO and Delft University of Technology, 1992.
11. Zielinski, A. J., Concrete under biaxial compressive-impact tensile loading. In *Fracture Toughness and Fracture Energy of Concrete*, ed. F. H. Wittman, Elsevier Science Publishers, Amsterdam, 1986, pp. 479–89.
12. Weerheijm, J., Reinhardt, H. W. & Postma, S., Experiments on concrete under lateral compression and tensile impact loading. In *Fracture Process in Concrete, Rock and Ceramics*, eds J. G. M. van Mier, J. G. Rots & A. Baker, E&F.N. Spon., London, 1991, pp. 839–48.
13. Tschegg, E. K., Kreuzer, H. & Elser, M., Mode I fracture behavior of concrete under biaxial loading. *J. of Material Science*, **30** (1995) 235–42.
14. RILEM Draft Recommendation (50-FMC), Determination of the fracture energy of mortar and concrete by means of three-point bending test on notched beams. *Materials and Science*, **18** (1985) 287–90.
15. Tschegg, E. K., Equipment and appropriate specimen shapes for tests to measure fracture values (in German). Patent No. 390328, patent application 31.1. 1986.
16. Tschegg, E. K., Load introduction equipment for fracture tests in brittle materials (in German). Patent No. 48, patent application 4.1. 1990.
17. Tschegg, E. K., New equipment for fracture tests on concrete. *Materialprüfung/Materials Testing*, **33** (1991) 338–43.
18. Brühwiller, E. & Wittmann, F. H., The wedge splitting test, a new method of performing stable fracture mechanics tests. *Eng. Frac. Mech.*, **35** (1–3) (1990) 117–25.
19. Guogan, Z., Hui Jiao & Shilang, X., Study of fracture behavior with wedge splitting test method. In *Fracture Process in Concrete, Rock and Ceramics*, eds J. G. M. van Mier, J. G. Rots & A. Baker, E&F.N. Spon., London, 1991, pp. 789–98.
20. Rokugo, K., Iwasa, M., Suzuki, T. & Koyanagi, W., Testing methods to determine tensile strain softening curve and fracture energy of concrete. In *Fracture Toughness and Fracture Energy*, ed. Mihahasi *et al.*, Balkema, Rotterdam, 1989, pp. 153–63.
21. Tschegg, E. K., Tan, T. M. & Stanzl, S. E., Development and experience with the wedge splitting test. *ASTM Testing and Evaluations*, submitted.
22. Tschegg, E. K. & Elser, M., Biaxial loading equipment for tests to measure fracture values (in German). Patent No. 390328, patent application 28.2, 1994.
23. Kreuzer, H., Tschegg, E. K. & Wilk, W., Fracture energy of concrete under biaxial loading. In *Proc. of the Int. Conf. on Dam Fracture*, eds V. Souma, R. Dungar & M. Moris, September 11–13 1991, Boulder, Colorado, USA, pp. 447–57.
24. Tschegg, E. K., Kreuzer, H. & Zelezny, M., Fracture in concrete under biaxial loading — numerical evaluation of wedge splitting test results. In *Proc. of the 1st Int. Conf. on Fracture Mechanics of Concrete Structure*, ed. Z. P. Bazant, June 1–5 1992, Breckenridge, Colorado, USA, pp. 455–60.
25. Elser, M., Bruchenergie und bruchmechanismen zementgebundener werkstoffe bei biaxialer belastung. MSc thesis, 1991, TU Wien, Austria.
26. Vonk, R. A., A micromechanical investigation of softening of concrete loaded in compression. *HERON*, **38** (3) (1993).
27. Irwin, G. R., Analyses of stresses and strains near the end of a crack traversing a plate. *J. of Applied Mechanics*, **24** (1957) 361–6.
28. Kotsovos, M. D. & Newman, J. B., Fracture mechanics and concrete behavior. *Magazine of Concrete Research (London)*, **33** (115) (1981).
29. Vonk, R. A., Influence of boundary conditions on softening of concrete loaded in compression. Report TUE-BKO-89.14, Eindhoven University of Technology, The Netherlands, 1989.
30. Vonk, R. A., Rutten, H. S., van Mier, J. G. M. & Fijneman, H. J., Influence of boundary conditions softening of concrete loaded in compression. In *Fracture of Concrete and Rock: Recent Developments*, eds S. P. Shah, S. E. Swartz & B. Barr, Elsevier Applied Science, London, pp. 711–20, 1989.
31. Van Mier, J. G. M. & Vonk, R. A., Fracture of concrete under multiaxial stress — recent developments, materials and structures. *RILEM*, **24** (1991) 61–5.
32. Hillerborg, A., Modeer, M. & Petersson, P. E., Analysis of formation and crack growth in concrete by means of fracture mechanics and finite elements. *Cement and Concrete Research*, **6** (1976) 773–82.
33. Lima, L. J., Violini, D. & Zerbino, R., Influence of water content on concrete strength under direct diametral tension. In *Fracture Toughness and Fracture Energy of Concrete*, ed. F. H. Wittmann, Elsevier Science Publishers, Amsterdam, 1986, pp. 219–22,
34. Bazant, Z. P., Size effect in blunt fracture — concrete, rock and metal. *J. Eng. Mech.*, **110** (1984) 518.
35. Hilsdorf, H. K. & Brameshuber, W., Probengrößenabhägigkeit bruchmechanischer kennwerte für Beton, Inst. f. Bauforschung RWTH Aachen, Festschrift. In *Baustoffe 1985*, Bauverlag Wiesbaden, 1985, pp. 62–72.